Modulation of radiative heating by the Madden-Julian Oscillation and convectively coupled Kelvin waves as observed by CloudSat

Ding Ma[1] and Zhiming Kuang[1,2]

Received 20 September 2011; revised 19 October 2011; accepted 20 October 2011; published 15 November 2011.

[1] The vertical distribution of radiative heating affects the moist static energy budget and potentially the maintenance and propagation of the Madden-Julian Oscillation (MJO). This paper uses CloudSat data to examine the radiative heating climatology in the tropics and the vertical structure of its modulation by the MJO and convectively coupled Kelvin Waves (KWs). Composites of active regions of the MJO and KW both show positive radiative heating anomaly in the middle and lower troposphere and slightly negative radiative heating anomaly in upper troposphere. Such bottom-heavy profiles can help to strengthen the MJO while weaken the KWs. Another finding is that cloud condensate anomalies associated with the MJO are significantly more bottom-heavy than those of the KWs, while the radiative heating anomalies associated with the MJO are only very slightly more bottom-heavy. **Citation:** Ma, D., and Z. Kuang (2011), Modulation of radiative heating by the Madden-Julian Oscillation and convectively coupled Kelvin waves as observed by CloudSat, *Geophys. Res. Lett.*, *38*, L21813, doi:10.1029/2011GL049734.

1. Introduction

[2] Although the Madden-Julian Oscillation (MJO) was first identified 40 years ago [*Madden and Julian*, 1971] and has long been recognized as an important phenomenon, it is still not well understood. The MJO features planetary scale circulation and convection signals in the tropics that propagate eastward at a speed of around 5 m/s. The convective signals of the MJO are clearly seen in the Outgoing Longwave Radiation (OLR) data, and its temperature, moisture and wind structures have been quite well documented [e.g., *Wheeler and Kiladis*, 1999; *Kiladis et al.*, 2005; *Zhang*, 2005]. Besides being the dominant intraseasonal variability in the tropics, the MJO also affects the El Nino-Southern Oscillation, tropical cyclones, Asian and Australian monsoons, and mid-latitude weather [e.g., *Zhang*, 2005]. The persistent difficulty in simulating the MJO with general circulation models highlights our insufficient knowledge of how the atmosphere operates in the tropics [e.g., *Lin et al.*, 2006; *Kim et al.*, 2009], and improved prediction and understanding of the MJO would also benefit weather and climate forecasts.

[3] A recently emerged view of the MJO is that, unlike the fundamentally buoyancy driven convectively coupled waves, processes that alter the column integrated moist static energy (MSE), are essential to the existence and the propagation characteristics of the MJO [e.g., *Raymond and Fuchs*, 2007; *Sobel et al.*, 2008; *Maloney*, 2009]. Radiative heating is known to be an important example of such a process. The extensive clouds in the active regions of the MJO, which have higher column-integrated MSE and enhanced convection, reduce the radiative cooling and help to amplify the original column MSE anomaly. Combining surface and top of the atmosphere radiative flux measurements, *Lin and Mapes* [2004] found that column integrated radiative heating anomaly is nearly in phase with the precipitation anomaly with a magnitude around 10–15% of the heating associated with the precipitation. Because column integrated radiative heating represents a net source of column integrated MSE, this amount is very significant, comparable to the amount of column MSE export associated with the divergent flow. Because of this importance, radiative feedback is invoked in a number of simple models of the MJO and the tropical mean circulation [e.g. *Raymond*, 2001; *Tian and Ramanathan*, 2003; *Bony and Emanuel*, 2005; *Sugiyama*, 2009].

[4] In addition to its column integral, the vertical distribution of radiative heating can also be important because it affects the efficacy of the circulation that arises in response to this radiative heating in importing or exporting column MSE. As briefly discussed by *Kuang* [2011] and confirmed by cloud-resolving model simulations, if the radiative heating is concentrated in the lower troposphere, the divergent circulation that arises to balance this heating results in more import of column MSE and further enhancement of convection. On the other hand, if the radiative heating is concentrated in the upper troposphere, the divergent circulation that arises results in more export of column MSE. Thus, for the same amount of column integrated radiative heating, a more bottom-heavy profile will result in a stronger response in the precipitation.

[5] The goal of this paper is to constrain the vertical distributions of radiative heating anomalies associated with the MJO using radiative heating profiles from CloudSat, which are derived from its multiyear global reflectivity measurements from the 94 GHz Cloud Profiling Radar (CPR) [*Stephens et al.*, 2002]. Previous studies have used CloudSat to examine cloud structures associated with the MJO and the boreal summer intraseasonal variabilities [*Masunaga et al.*, 2008; *Riley et al.*, 2011; *Jiang et al.*, 2011]. In addition to results for the MJO, we will also present the results for convectively coupled Kelvin waves (KWs). While radiative feedback is not believed to be essential for the existence of convectively coupled waves [e.g., *Mapes*, 2000; *Khouider*

[1]Department of Earth and Planetary Science, Harvard University, Cambridge, Massachusetts, USA.
[2]School of Engineering and Applied Sciences, Harvard University, Cambridge, Massachusetts, USA.

0094-8276/11/2011GL049734

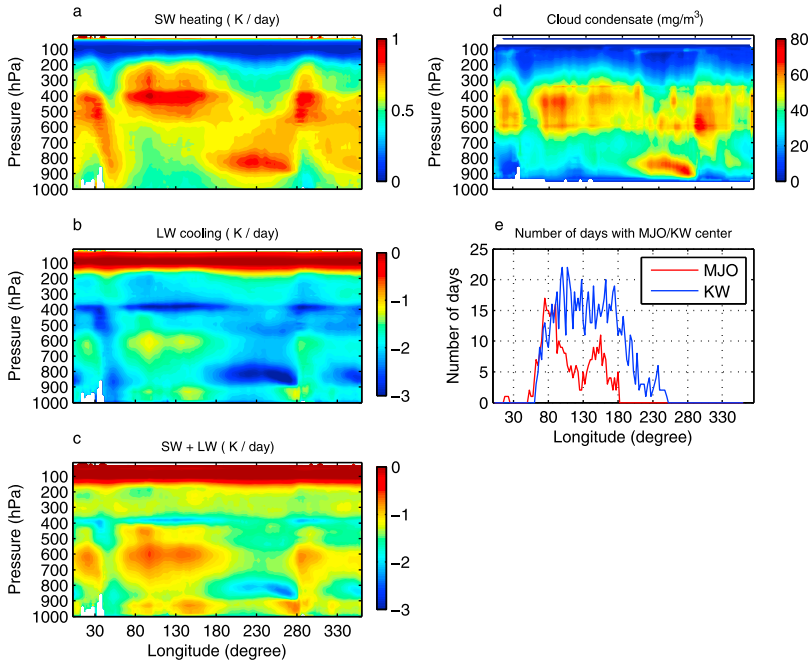

Figure 1. The 4-year climatology of radiative heating averaged between 10°S and 10°N (a) SW, (b) LW, (c) total radiative heating, (d) total cloud water content, and (e) the number of days for which the identified active centers of the MJO/KWs fall in a particular 2.5° longitude bin.

and Majda, 2006; *Kuang*, 2008a, 2008b; *Andersen and Kuang*, 2008], how radiative heating is distributed vertically could still modify the characteristics of these waves.

2. Data and Method

[6] We use radiative heating, cloud water/ice, water vapor and temperature data from CloudSat. The level 2 radiative fluxes and heating rates algorithm (2B-FLXHR) of CloudSat produces vertically resolved radiative heating data set based on the results from CloudSat's CPR. Cloud water/ice content data is provided by the level 2 radar-visible optical depth cloud water content product (2B-CWC-RVOD), using a combination of measured radar reflectivity factor and estimates of visible optical depth. Radiation and cloud data from Sep. 1, 2006 to Aug. 31, 2010 are used. We also analyzed temperature and water vapor data contained in the ECMWF-AUX product of CloudSat, which is derived from the European Center for Medium-Range Weather Forecasts reanalysis. Temperature and moisture structures associated with the MJO have been extensively documented before [e.g., *Kiladis et al.*, 2005; *Tian et al.*, 2006] and are included here only for reference. Only one year of the temperature and water vapor data (from Sep. 1, 2006 to Aug. 31, 2007) was used, which already yielded clear signals for our purpose. We shall use the 2.5° latitude × 2.5° longitude global NOAA Interpolated daily mean outgoing Longwave Radiation (OLR) dataset to identify the MJO and Kelvin wave events.

[7] A major limitation of this work is that radiative heating and cloud condensate are derived products instead of raw measurements such as the radar reflectivity. The cloud condensate products are retrieval results based on a priori lognormal size distributions constrained by the measured radar reflectivity. The products also have issues in heavily precipitating scenes because of radar attenuation and deviations from log-normality. The radiation fields are results from further radiative transfer calculations based on the cloud condensate values and reanalyzed temperature and moisture data. Despite these uncertainties, the CloudSat data represent our best current estimates of global cloud condensate and radiative heating rate distributions and it is worthwhile to have a first look at the modulations of these fields by the MJO and the KWs. Furthermore, atmospheric layers with heavy precipitation are in general already optically opaque so that radiative heating rates there are not sensitive to changes/errors in the cloud condensate retrievals, as we have verified in offline radiative transfer calculations. One might also reasonably expect differences seen between the composite structures of the MJO and the KWs to be less sensitive to the aforementioned uncertainties.

[8] To construct the MJO composite, we first average OLR data along the equator (between 10°S and 10°N), and then filter the data according to the space-time spectral window of the MJO (zonal wavenumber 0.5–9.5, frequency 0.01–0.05), following the approach of *Wheeler and Kiladis* [1999]. For each day, the local minima of the filtered OLR with values less than −20 W/m^2 are identified, and labeled as the "active convective centers". CloudSat data within 10°N/S are then binned according to their relative position to the active convective center of the MJO on the day they were collected to produce a composite structure. KWs composites are constructed similarly. With this simple procedure, we have neglected regional differences in MJO and KW structures.

3. Results

[9] To provide a context for the anomalies to be discussed, we present in Figure 1 the 4-year (Sep. 1, 2006–Aug 31, 2010) averages of (a) shortwave (SW), (b) longwave

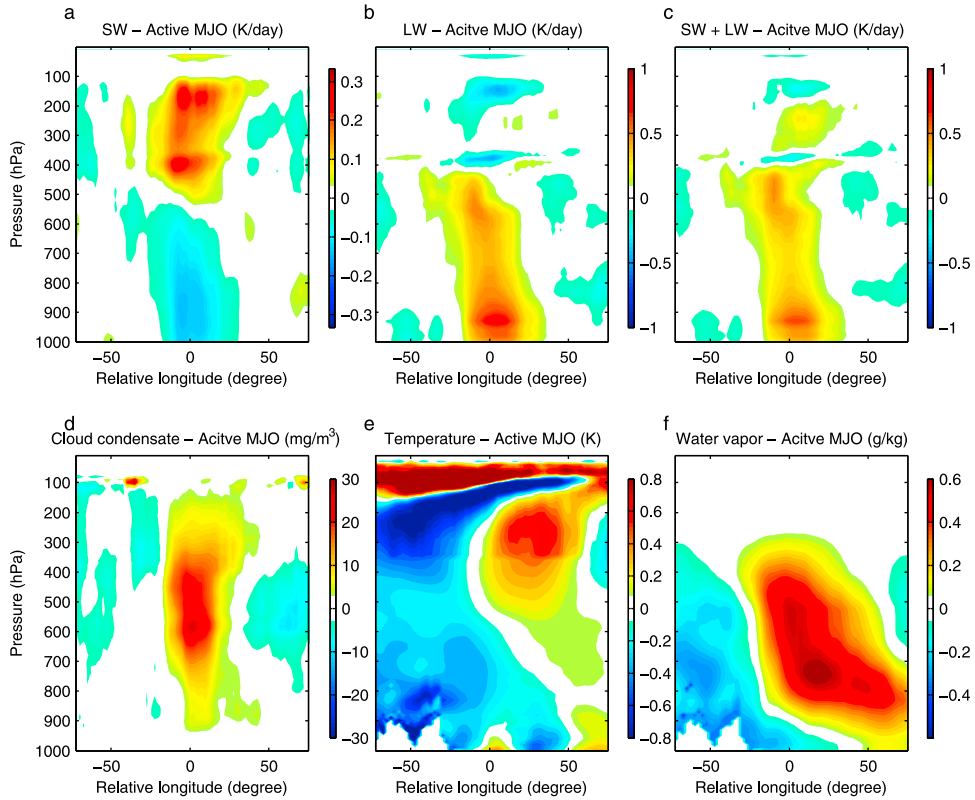

Figure 2. The vertical-longitudinal distributions of anomalous (a) SW, (b) LW, (c) total radiative heating, (d) total cloud water, (e) temperature, and (f) water vapor associated with the MJO.

(LW), (c) total radiative heating rates, (d) total cloud water content averaged between 10°N/S and shown as a function of longitude (we have diurnally averaged the data and applied a 10°- longitude moving average). In Figure 1e, we also show the number of days for which the identified active convective centers of the MJO/KWs fall in a particular 2.5° longitude bin. Note that even though there are higher frequencies of convective centers associated with the KWs, the MJO is more influential because the MJO anomalies span a wider range in space. The active centers mostly reside over the Indian Ocean and the western Pacific Ocean. The climatology of cloud water content is consistent with previous studies [e.g., *Waliser et al.*, 2009]. The strong impact of the time-mean cloudiness is apparent in the radiative heating climatology. Over the Indian Ocean, west Pacific Ocean and the Amazon, because of active deep convection in these regions, there is abundant cloud water between 400 hPa to 600 hPa, with a maximum cloud water content around 60 mg/m^3. In these regions, daily mean SW heating is strongest in the upper troposphere and peaks at around 1 K/day around 400-hPa. Over the central and eastern Pacific, cloud water is concentrated below 700 hPa, because this region is dominated by shallow stratus clouds, and the daily mean SW heating peaks around 1 K/day between 700 hPa and 900 hPa. Such spatial patterns are due to SW absorption by cloud condensates. Similarly, the LW radiative heating distributions also show strong imprints of clouds, because of the strong emissivity of clouds compared to clear sky atmosphere. The maximum LW cooling at the top of the stratus clouds over the eastern Pacific Ocean reaches −3 K/day. Deep convective clouds over the warm pool strengthen the LW cooling around 400 hPa, also reaching −3 K/day, while weakening the LW cooling rates in the midtroposphere to −1.3 K/day. Overall, the LW cooling is stronger than the SW heating so that total radiative cooling distribution to a large extent resembles that of the LW cooling. These results are generally consistent with previous estimates [e.g., *L'Ecuyer and McGarragh*, 2010].

[10] Within active MJO regions, deep convection is enhanced. SW heating (Figure 2a) increases by around 30% above 500 hPa. There are two peaks of positive SW heating anomalies, one near 400 hPa and another near 200 hPa, the latter being the main detrainment level of anvils, and the peak values reach 0.3 K/day. Below 500 hPa is a negative SW heating anomaly of around −0.1 K/day. The signals extend 20 degrees east and west of the convective center. Patterns of LW anomalies (Figure 2b) are similar to those of SW except with the opposite signs. LW cooling increases by 0.5 K/day near 400 hPa and at 150 hPa. The decreased LW cooling below 400 hPa is more bottom-heavy than that of the climatology, with a maximum of 0.9 K/day at 900 hPa. The total radiative heating anomaly (Figure 2c) is dominated by LW anomalies. Active MJO reduces radiative cooling in the column, with a peak of 0.7 K/day near the cloud base (~930 Pa). When we integrate the data vertically, the column integrated radiative heating anomaly peaks at around 20 W/m^2 near the active convective center of the MJO.

[11] The stronger convection is apparent in the anomalous cloud water content (Figure 2d). Cloud water increases by around 50%, peaking at 30 mg/m^3 between 500 hPa and

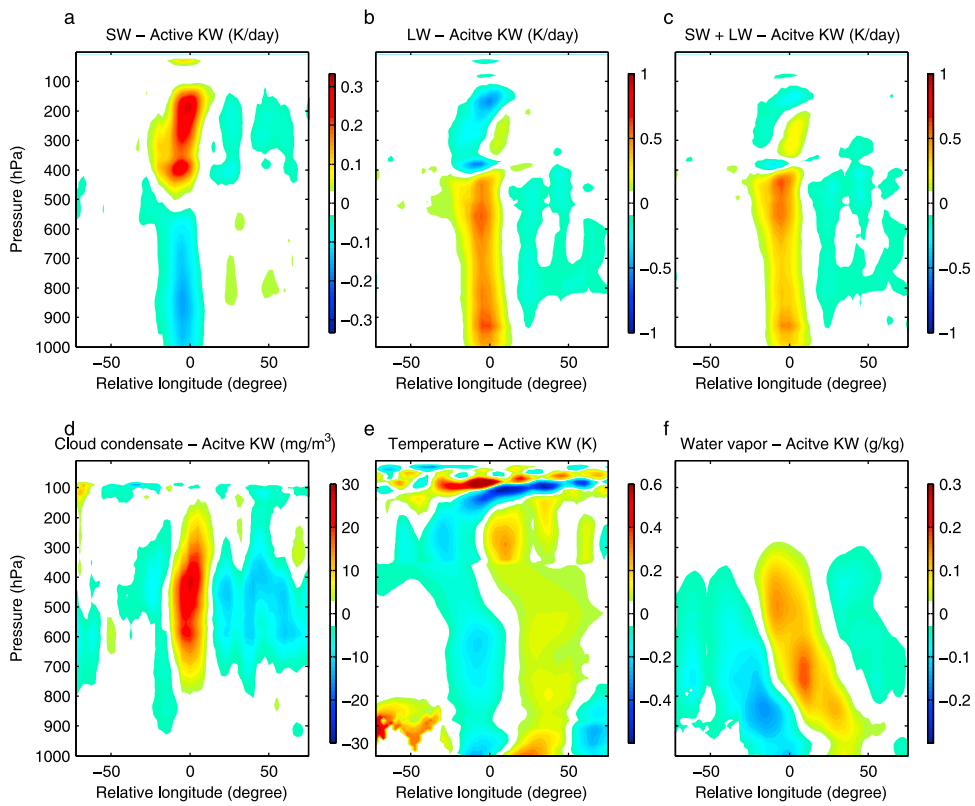

Figure 3. Same as Figure 2, but for the KWs.

600 hPa. It is interesting to note that there is not a vertical tilt in the cloud condensate anomalies that is often associated with the MJO cloud fields [e.g., *Benedict and Randall*, 2007]. The total anomalous cloud water signal extends from 900 hPa to 100 hPa and shows a middle-heavy profile, indicating a greater increase of mid-level clouds compared to the climatology. Because radiation is derived from cloud water, the distribution of cloud water is consistent with the pattern of radiation anomalies. Additional clouds absorb more solar radiation. This increases SW heating in the upper troposphere while reducing the solar radiation reaching the lower troposphere, decreasing the SW heating there. Meanwhile, cloud water is a stronger LW emitter than clear sky air so LW radiative cooling increases above 450 hPa, while radiative cooling decreases below that level because of the enhanced greenhouse effect. We have also constructed meridional composites (figures not shown) and similar characteristics are observed. The width of MJO signal in latitude is closely related to the width of the ITCZ.

[12] Composite structures of temperature and water vapor are shown in Figures 2e and 2f for reference. The temperature structure (Figure 2e) shows the well-known boomerang shape, while the water vapor anomalies tilt westward with height, both consistent with previous studies [e.g., *Kiladis et al.*, 2005; *Tian et al.*, 2006].

[13] The KWs composite structures are similar to those of the MJO except the following differences. Because the KWs have shorter zonal wavelengths than the MJO, the signal for KWs is narrower, covering only 20° in longitude compared to 50° with the MJO. More importantly, KWs are also different from the MJO in that the total radiative heating (Figure 3c) and cloud water (Figure 3d) anomaly profiles of KWs are less bottom-heavy as compared to the MJO (Figure 2c). Anomalous temperature (Figure 3e) and water vapor (Figure 3f) for the KWs are broadly similar to those of the MJO and consistent with previous studies [e.g., *Straub and Kiladis*, 2002].

[14] To further illustrate the difference between the MJO and the KW composites, we show the radiative heating (Figure 4a) and cloud water condensate (Figure 4b) profiles averaged over the 10° longitude around the reference points of the MJO (red) and KWs (blue) composites. The profiles are normalized so all values squared sum to one. Results from two 2-year subsets of the data are shown (dashed lines) to give an indication of the robustness of the results. The MJO has a clearly more bottom-heavy profile in terms of cloud water, which peaks at 600 hPa, 200 hPa lower than that from the KWs. The profile of radiative heating anomalies associated with the MJO is also more bottom-heavy than the KWs', but only very slightly. We note that Figure 1e shows that the MJO and KW events that were used to produce the composites have similar spatial distributions. If anything, there are more KW events over the central Pacific, where the climatological radiative heating and cloud water profiles are more bottom-heavy. Therefore, the difference between the MJO and the KW profiles are not from biased samplings of the different local climatology. The difference in radiative heating anomalies is smaller, likely because the cloud condensate anomalies are mostly from scenes with heavy precipitation, where the atmosphere, especially the

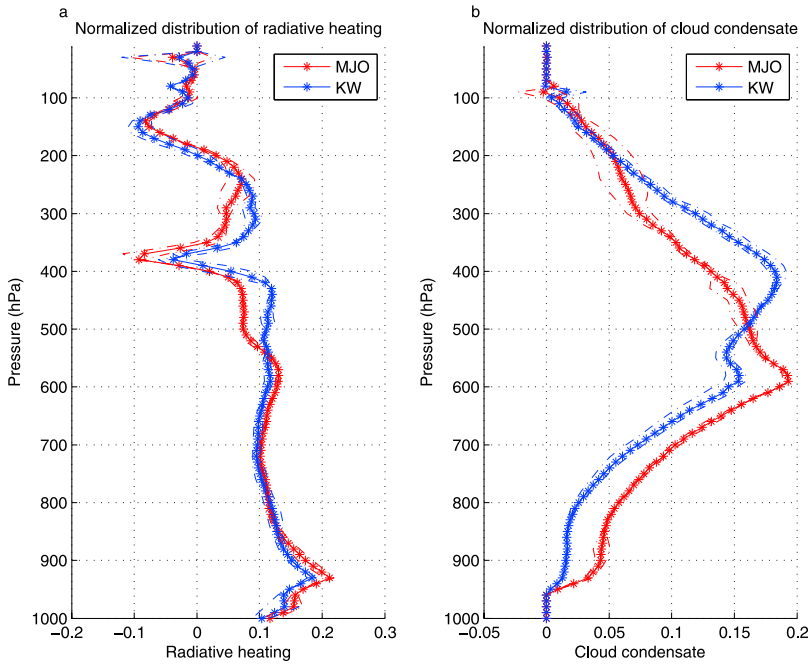

Figure 4. (a) Normalized vertical distribution of radiative heating and (b) total cloud water content. The solid red and blue with stars are for the MJO and KWs anomalies respectively, using the full 4-year dataset. The dashed lines are results from two 2-year-long subsets of the data.

lower troposphere, is already optically opaque so that radiative heating is insensitive to cloud condensate amount.

4. Discussions and Summary

[15] We have used data from CloudSat, the first space-based observations of vertical cloud distributions and radiative heating profiles derived from these observations and radiative transfer calculations, to examine the modulation of radiative heating by the MJO and convectively coupled Kelvin waves. We first briefly described the climatology of radiative heating in the tropics, which shows strong imprints by clouds. Using the OLR data to identify MJO and KW events, we then made composite structures of radiative heating, cloud condensates, temperature, and water vapor for the MJO and KWs. Temperature and water vapor signals from the composites are consistent with previous studies [e.g., *Straub and Kiladis*, 2002; *Kiladis et al.*, 2005; *Zhang*, 2005; *Tian et al.*, 2006]. In actively convecting regions of the MJO and the KWs, SW heating is enhanced in the upper troposphere (above 400 hPa) and reduced in the middle and lower troposphere. LW heating anomalies show a pattern of the opposite sign with larger amplitude. As a result, the total radiative heating anomaly is positive in the middle and lower troposphere and slightly negative in the upper troposphere. Such radiative heating anomaly profiles can affect the dynamics of the MJO and the KWs. Besides the net input of column MSE due to the radiative heating, the divergent circulation that arises in response to a bottom-heavy radiative heating anomaly will also be bottom-heavy, which results in more import of column MSE and further enhancement and maintenance of column MSE anomalies associated with the MJO. On the other hand, the bottom-heavy radiative heating profile counters the top-heavy stratiform heating that convectively coupled waves rely on and can act to weaken such waves. The results presented in Figure 4 thus help to quantify this bottom-heaviness and its impact on the MJO and KWs. In a recent paper [*Andersen and Kuang*, 2011], it was reported that when the radiative heating feedback is disabled, convectively coupled waves are strengthened while MJO-like disturbances are weakened, consistent with the above expectations.

[16] There are also intriguing differences between the MJO and KWs. The more bottom-heavy vertical structure of the MJO is seen clearly in the cloud condensate field. It was argued by *Kuang* [2011], based on cloud-system resolving model results and theoretical arguments, that for longer wavelength quasi-steady disturbances, the temperature anomalies required to drive the divergent flow become significant and will force convection to become more bottom-heavy. The finding that the MJO composite radiative heating anomaly is more bottom-heavy than that of convectively coupled KWs is consistent with this argument. Additional studies (observational and numerical) are warranted to further test this idea.

[17] **Acknowledgments.** The research was supported by NSF grant AGS-1062016 and DOE grant DE-FG02-08ER64556 as part of the Atmospheric System Research (ASR) program. The authors thank Adam Sobel and an anonymous reviewer for very constructive and helpful reviews, Joe Andersen for valuable codes to start this study and helpful discussions, Mary Moore and Baijun Tian for valuable comments, and the Harvard FAS Science Division Research Computing Group for computing support.

[18] The Editor thanks the two anonymous reviewers for their assistance in evaluating this paper.

References

Andersen, J. A., and Z. Kuang (2008), A toy model of the instability in the equatorially trapped convectively coupled waves on the equatorial beta plane, *J. Atmos. Sci.*, *65*, 3736–3757, doi:10.1175/2008JAS2776.1.

Andersen, J. A., and Z. Kuang (2011), Moist Static Energy Budget of MJO-like disturbances in the atmosphere of a zonally symmetric aquaplanet, *J. Clim.*, in press.

Benedict, J. J., and D. A. Randall (2007), Observed characteristics of the MJO relative to maximum rainfall, *J. Atmos. Sci.*, *64*, 2332–2354, doi:10.1175/JAS3968.1.

Bony, S., and K. A. Emanuel (2005), On the role of moist processes in tropical Intraseasonal variability: Cloud–radiation and moisture–convection feedbacks, *J. Atmos. Sci.*, *62*, 2770–2789, doi:10.1175/JAS3506.1.

Jiang, X., D. E. Waliser, J.-L. Li, and C. Woods (2011), Vertical structures of cloud water associated with the boreal summer intraseasonal oscillation based on CloudSat observations and ERA-Interim reanalysis, *Clim. Dyn.*, *36*, 2219–2232, doi:10.1007/s00382-010-0853-8.

Khouider, B., and A. J. Majda (2006), A simple multicloud parameterization for convectively coupled tropical waves. Part I: Linear analysis, *J. Atmos. Sci.*, *63*, 1308–1323, doi:10.1175/JAS3677.1.

Kiladis, G. N., K. H. Straub, and P. T. Haertel (2005), Zonal and vertical structure of the Madden-Julian Oscillation, *J. Atmos. Sci.*, *62*, 2790–2809, doi:10.1175/JAS3520.1.

Kim, D., et al. (2009), Application of MJO simulation diagnostics to climate models, *J. Clim.*, *22*, 6413–6436, doi:10.1175/2009JCLI3063.1.

Kuang, Z. (2008a), Modeling the interaction between cumulus convection and linear gravity waves using a limited-domain cloud system-resolving model, *J. Atmos. Sci.*, *65*, 576–591, doi:10.1175/2007JAS2399.1.

Kuang, Z. (2008b), A moisture-stratiform instability for convectively coupled waves, *J. Atmos. Sci.*, *65*, 834–854, doi:10.1175/2007JAS2444.1.

Kuang, Z. (2011), The wavelength dependence of the gross moist stability and the scale selection in the instability of column integrated moist static energy, *J. Atmos. Sci.*, *68*, 61–74, doi:10.1175/2010JAS3591.1.

L'Ecuyer, T. S., and G. McGarragh (2010), A 10-year climatology of tropical radiative heating and its vertical structure from TRMM observations, *J. Clim.*, *23*, 519–541, doi:10.1175/2009JCLI3018.1.

Lin, J., and B. Mapes (2004), Radiation budget of the tropical intraseasonal oscillation, *J. Atmos. Sci.*, *61*, 2050–2062, doi:10.1175/1520-0469(2004)061<2050:RBOTTI>2.0.CO;2.

Lin, J.-L., et al. (2006), Tropical intraseasonal variability in 14 IPCC AR4 climate models. Part I: Convective signals, *J. Clim.*, *19*, 2665–2690, doi:10.1175/JCLI3735.1.

Madden, R., and P. Julian (1971), Detection of a 40–50 Day Oscillation in the Zonal Wind in the Tropical Pacific, *J. Atmos. Sci.*, *28*, 702–708.

Maloney, E. D. (2009), The moist static energy budget of a composite tropical intraseasonal oscillation in a climate model, *J. Clim.*, *22*, 711–729, doi:10.1175/2008JCLI2542.1.

Mapes, B. E. (2000), Convective inhibition, subgridscale triggering, and stratiform instability in a toy tropical wave model, *J. Atmos. Sci.*, *57*, 1515–1535, doi:10.1175/1520-0469(2000)057<1515:CISSTE>2.0.CO;2.

Masunaga, H., M. Satoh, and H. Miura (2008), A joint satellite and global cloud-resolving model analysis of a Madden-Julian Oscillation event: Model diagnosis, *J. Geophys. Res.*, *113*, D17210, doi:10.1029/2008JD009986.

Raymond, D. J. (2001), A new model of the Madden-Julian Oscillation, *J. Atmos. Sci.*, *58*, 2807–2819, doi:10.1175/1520-0469(2001)058<2807:ANMOTM>2.0.CO;2.

Raymond, D. J., and Z. Fuchs (2007), Convectively coupled gravity and moisture modes in a simple atmospheric model, *Tellus, Ser. A*, *59*, 627–640, doi:10.1111/j.1600-0870.2007.00268.x.

Riley, E., B. Mapes, and S. Tulich (2011), Clouds associated with the Madden-Julian Oscillation: A new perspective from CloudSat, *J. Atmos. Sci.*, doi:10.1175/JAS-D-11-030.1, in press.

Sobel, A., E. Maloney, G. Bellon, and D. Frierson (2008), The role of surface heat fluxes in tropical intraseasonal oscillations, *Nat. Geosci.*, *1*, 653–657, doi:10.1038/ngeo312.

Stephens, G. L., et al. (2002), The CloudSat mission and the A-Train, *Bull. Am. Meteorol. Soc.*, *83*, 1771–1790, doi:10.1175/BAMS-83-12-1771.

Straub, K. H., and G. N. Kiladis (2002), Observations of a convectively coupled Kelvin wave in the eastern Pacific ITCZ, *J. Atmos. Sci.*, *59*, 30–53, doi:10.1175/1520-0469(2002)059<0030:OOACCK>2.0.CO;2.

Sugiyama, M. (2009), The moisture mode in the quasi-equilibrium tropical circulation model. Part I: Analysis based on the weak temperature gradient approximation, *J. Atmos. Sci.*, *66*, 1507–1523, doi:10.1175/2008JAS2690.1.

Tian, B., and V. Ramanathan (2003), A simple moist tropical atmosphere model: The role of cloud radiative forcing, *J. Clim.*, *16*, 2086–2092, doi:10.1175/1520-0442(2003)016<2086:ASMTAM>2.0.CO;2.

Tian, B., D. E. Waliser, E. J. Fetzer, B. H. Lambrigtsen, Y. Yung, and B. Wang (2006), Vertical moist thermodynamic structure and spatial-temporal evolution of the MJO in AIRS observations, *J. Atmos. Sci.*, *63*, 2462–2485, doi:10.1175/JAS3782.1.

Waliser, D., et al. (2009), Cloud ice: A climate model challenge with signs and expectations of progress, *J. Geophys. Res.*, *114*, D00A21, doi:10.1029/2008JD010015.

Wheeler, M., and G. Kiladis (1999), Convectively coupled equatorial waves: analysis of clouds and temperature in the wavenumber–frequency domain, *J. Atmos. Sci.*, *56*, 374–399, doi:10.1175/1520-0469(1999)056<0374:CCEWAO>2.0.CO;2.

Zhang, C. (2005), Madden-Julian Oscillation, *Rev. Geophys.*, *43*, RG2003, doi:10.1029/2004RG000158.

Z. Kuang and D. Ma, Department of Earth and Planetary Science, Harvard University, 20 Oxford St., Cambridge, MA 02138, USA. (dingma@fas.harvard.edu)